Apparent vanishing of ferroelectricity in nanostructured BiScO3PbTiO3

H Amorín, R Jiménez, J Ricote, Teresa Hungría, A Castro, M Algueró

Apparent vanishing of ferroelectricity in nanostructured $BiScO_3$-$PbTiO_3$

H. Amorín, R. Jiménez, J. Ricote, T. Hungría, A. Castro and M. Algueró

Instituto de Ciencia de Materiales de Madrid, CSIC. Cantoblanco, 28049 Madrid, Spain

Abstract

Nanostructured ceramics of high-temperature piezoelectric $0.375BiScO_3$-$0.625PbTiO_3$ were prepared by spark plasma sintering of nanocrystalline powders obtained by mechanosynthesis. The macroscopic electrical properties were characterized on dense ceramics with decreasing average grain size down to 28 nm. Results indicate that the electric field is screened by the electrically insulating grain boundaries at the nanoscale, which needs to be considered when discussing size effects in ferroelectric polycrystalline materials. Moreover, the requirement of increasingly large electric fields to achieve a given polarization with the decrease of the grain size, together with the depletion of the dielectric anomaly associated with the ferroelectric transition until its disappearance, seems to be the result of grain boundary effects.

1. Introduction

Piezoelectric devices are not oblivious to the current miniaturization trend in the ceramic technologies for microelectronics, which demand functional materials with submicron or even nanometric grain size for reliability [1]. The feasibility of the miniaturized technologies depends on how functional properties, such as polarization switching, retention, and piezoelectricity, behave with the grain size reduction to the nanoscale [2]. This has raised an interest for studying grain size effects in ferroelectric polycrystals [3-5], and, among them, specifically in perovskite morphotropic phase boundary (MPB) materials [6-10], as they have shown very high piezoelectric activity. These materials are good candidates to implement piezoelectric sensing and actuation in a range of anticipated micro- and nanotechnologies.

Previous studies in MPB materials were focused on relaxor-based solid solutions with the highest piezoelectric coefficients reported in single-crystals, i.e., $Pb(Mg_{1/3}Nb_{2/3})O_3$-$PbTiO_3$ and $Pb(Zn_{1/3}Nb_{2/3})O_3$-$PbTiO_3$. It has been found the stabilization of the high-temperature relaxor state for nanostructured ceramics, indicating that the long range ferroelectric order does not develop in the nanoscale [6-10]. However, a similar in-depth study of a non-relaxor MPB material with high piezoelectric activity down to the nanoscale has not been reported yet, though there have been some studies in $Pb(Zr,Ti)O_3$ and some lead-free materials with grain sizes at the submicron range [11-13].

$BiScO_3$-$PbTiO_3$ is a non-relaxor MPB material that exhibits high Curie temperature (T_C) and large piezoelectric coefficients (d_{33}) as compared with $Pb(Zr,Ti)O_3$ [14, 15]. The broad range of usage temperatures, up to ~350 ºC, makes this material promising for the next generation of high-temperature and high-power piezoelectric devices [16]. The (1-*x*)$BiScO_3$-*x*$PbTiO_3$ solid solution has a wide MPB region ($0.6 < x < 0.7$), in which monoclinic *Cm* and tetragonal *P*4*mm* polymorphs coexist [17]. Furthermore, a recent work indicates that *Cm* symmetry persists in nanocrystals with very small sizes [18]. Large piezoelectric properties

have been reported in fine-grained ceramics in which grain growth was restricted to the submicron range [19, 20].

First results on nanostructured ceramics of MPB $BiScO_3$-$PbTiO_3$ have shown polarization switching and radial piezoelectric resonance after poling [21], thus demonstrating macroscopic functionality and better down-scaling behavior than that of relaxor-based MPB materials. In this work, we report macroscopic properties of $0.375BiScO_3$-$0.625PbTiO_3$ (BSPT) ceramics with decreasing grain size from the submicron range down to the nanoscale. Results clearly indicate that grain size effects alone cannot account for the observed phenomenology, and that grain boundaries may play a dominant role for the smallest sizes.

2. Experimental procedure

Highly dense, submicron- and nanostructured BSPT ceramics with composition in the MPB region (x = 0.625) were prepared by spark plasma sintering (SPS, 2080 Sumitomo apparatus) of a nanocrystalline powder obtained by mechanosynthesis. The powder with the nominal composition was obtained by mechanochemical activation of the binary oxides in oxygen atmosphere using a high-energy planetary mill. Details of the procedures and of the mechanisms taking place during the mechanosynthesis can be found elsewhere [22]. The powder presented an average particle size of 11 nm, as measured by transmission electron microscopy (TEM, Philips CM20FEG microscope working at 200 kV) [22]. SPS conditions were tailored for obtaining ceramics with a range of grain sizes in the submicron and nanometric ranges. This technique allows high densification at moderate temperatures and short times, thus limiting grain growth, as described elsewhere [23]. Results here shown correspond to ceramics sintered at 650 and 800 ºC under uniaxial pressures of 75 and 120 MPa during 3 min (see Table 1). Besides, results on a coarse grain ceramic prepared from the same powder by conventional sintering at 1100 ºC during 1 h are also shown for comparison.

Figure 1 shows an example of a typical TEM image and the grain size distribution of the BSPT ceramic with an average grain size of 28 nm. The Feret's diameters of more than 150 grains were measured on TEM or scanning electron microscopy images of the nanostructured and submicron-grain ceramics, respectively, to obtain reliable size distributions. Lognormal distributions were found for all SPS ceramics, whose average grain sizes (*G*) are given in Table 1. Perovskite single phase materials were confirmed by X-ray diffraction (XRD, Siemens D500 diffractometer with Cu K_α radiation) in all cases, as shown in figure 2. Density was obtained by the Archimedes' method, and densification levels above 98% of the theoretical density were achieved after SPS for all SPS ceramics.

Electrical characterization was carried out on ceramic discs on which Pt/Au electrodes were deposited by sputtering and annealed at 500 ºC in air. Dielectric permittivity and losses were dynamically measured at a heating rate of 1.5 ºC min^{-1} using a HP4284A precision LCR Meter in the frequency range from 100 Hz to 1 MHz. In addition, impedance measurements were carried out in static mode with temperature steps of 20 ºC after 30 min of stabilization in the frequency range from 20 Hz to 1 MHz. Room temperature ferroelectric P-E hysteresis loops were obtained by current integration. Low frequency (0.1 Hz), high voltage sine waves were applied by the combination of a synthesizer/function generator (HP3325B) and a high-voltage amplifier (Trek 10/40A), while charge was measured with a homebuilt charge to voltage converter. Loops are presented after compensation by subtracting the linear polarization and conduction contributions assuming a resistor and a capacitor in parallel. For piezoelectric measurements the ceramics were poled in an oil bath at 100 ºC under a field of 40 $kVcm^{-1}$ for 15 min, which are standard conditions for coarse grain ceramics [14, 20, 22], and the d_{33} coefficient was measured using a Berlincourt piezo meter.

Local piezoelectric measurements were carried out by piezoresponse force microscopy (PFM, Nanotec® with WSxM® software) using conductive Pt/Ir coated tips on cantilevers with a force constant of 42 N/m, to apply an *ac* voltage of 1 V at 50 kHz.

3. Results and discussion

Figures 3 and 4 show the temperature dependence of the relative dielectric permittivity (K') and losses (tan δ), respectively, for the SPS ceramics under study at several frequencies, in which a low-frequency dispersion is observed in the temperature range where the dielectric anomaly associated with the transition from the ferroelectric to the paraelectric state occurs for this composition; T_C ~465 ºC. It must be taken into account that the high-temperature dielectric response of ferroelectric polycrystals usually consists of several contributions that include Debye-type relaxation processes, which often appear in perovskite-type oxides and are attributed to defects in the materials, e.g., short range hopping of oxygen vacancies [24]. Reducing conditions within the graphite die during the SPS experiment might promote the formation of these defects [25]. Nevertheless, a size effect in the ferroelectric transition is evident in the curves obtained at 1 MHz, a frequency at which the relaxation has shifted well above T_C. The dielectric anomaly associated with the ferroelectric transition is still present at 442 ºC for the nanostructured ceramic with G = 80 nm, yet strongly flattened and broadened. This effect has been already observed in both relaxor-based and non-relaxor MPB materials [6, 8, 11, 12, 26]. However, the ferroelectric transition cannot be discerned from the curve of the nanostructured ceramic with the smallest grain size, G = 28 nm.

Figure 5(a) shows the P-E hysteresis loops for the ceramics under study along with that obtained for the coarse grain ceramic for comparison. A square loop close to saturation was obtained for the coarse grain ceramic, as confirmed by the curves of spontaneous (P_s) and remnant polarization (P_r) against maximum applied electric field in figure 5(b). Macroscopic

ferroelectricity was also found in the nanostructured ceramics with decreasing grain size down to G = 80 nm, while polarization switching was not observed for the material with G = 28 nm, for which a typical linear dielectric behavior was observed. Both spontaneous and remnant polarizations continuously decrease with the decrease of the grain size and the loops become increasingly leant. Curves in figure 5(b) indicate that saturation is far from being reached in the case of the nanostructured ceramics. Note that the electric field derivative of the spontaneous polarization continuously decreases above 40 $kVcm^{-1}$ for the coarse grain ceramic, indicating that saturation is slowly approached, but it is still increasing at the highest measured electric fields for all the SPS ceramics. These derivatives strongly suggest that materials progressively move away from saturation with the decrease of the grain size. Unfortunately, saturation cannot be reached before dielectric breakdown in these ceramics.

The occurrence of macroscopic ferroelectric switching indicates that the nanostructured ceramics can be poled, and their piezoelectric properties studied. Significant variations of the d_{33} coefficient with decreasing grain size were found (see Table 1). On the one hand, a relatively high d_{33} of 110 pC/N was obtained for the ceramic with G = 375 nm, which has to be compared with the 150 pC/N reached in the coarse grain ceramic (note that x = 0.625, though in the MPB region, is not the composition for which d_{33} peaks reaching ~350 pC/N). However, a low d_{33} of 24 pC/N was measured for the ceramic with G = 80 nm, and only 2 pC/N was achieved for the ceramic with G = 28 nm. These values show the reduced but measurable piezoelectricity of the nanostructured ceramics.

The grain size effects observed on the spontaneous polarization and the d_{33} coefficient are accompanied by a significant increase of the total resistivity (ρ) of the SPS ceramics with the decrease of the grain size. In electroceramics and typically in ferroelectrics, the resistance of grain boundaries exceeds that of the grains [27]. Therefore, it is expected in this case an increase of the total resistivity for nanostructured ceramics due to their larger volume fraction

of insulating grain boundaries. This seems to be the case for the BSPT ceramics under study, for which the resistivity calculated from the low-field hysteresis loops at 0.1 Hz; i.e., under subcoercive conditions at which the material behaves as a lossy linear dielectric, and assuming a parallel RC circuit, increases about 3 times from the coarse grain ceramic to the nanostructured ceramic with G = 80 nm (see Table 1). Moreover, very large resistivity of ~10^{12} Ω·cm was measured for the material with G = 28 nm, which is two orders of magnitude larger than that obtained for the coarse grain ceramic, suggesting an even larger contribution of the electrically insulating grain boundaries to the total resistivity for this ceramic.

Figure 6(a) shows the temperature dependence of the total *dc* conductivity (σ_{dc}) for the ceramics under study obtained by circuit analysis of the impedance spectroscopy data. Similar Arrhenius dependences were observed for the coarse grain ceramic and the nanostructured ceramics with decreasing grain size down to 80 nm, for which a change of slope at ~300 ºC is observed. Above this temperature, activation energy (E_a) of ~1.1 eV is obtained, typical of mobile doubly-ionized oxygen vacancies ($V_{\ddot{O}}$) [24], which can also be responsible of the dipolar high-temperature relaxation observed in the dielectric curves. Below 300 ºC, a change in the Arrhenius behavior with activation energy of ~0.6 eV indicates a change in the mechanism dominating *dc* conductivity, in which predominant charge carriers in this case could be electrons linked to the doubly-ionized oxygen vacancies [24].

The *ac* conductivity (σ_{ac}) of all ceramics under study displays two contributions at low and high frequencies in the temperature range between 200 and 500 ºC, as shown in figure 6(b) for the ceramic with G = 375 nm (small arrows indicate the approximate position of the high frequency contribution to conductivity for different temperatures), which are usually associated with the grain boundary and bulk responses, respectively [27-29]. This indicates that the grain boundaries (low frequency contribution) dominate the total *dc* conductivity.

However, the temperature dependence of the total *dc* conductivity for the nanostructured ceramic with the smallest grain size, *G* = 28 nm, shows a different behavior. In this case, only the high-temperature mechanism with activation energy of ~1.4 eV is observed in all the temperature range. The higher activation energy and the lower total *dc* conductivity obtained for this ceramic may be explained by considering a mechanism of association of defects at the grain boundaries, which reduces the mobility of the doubly-ionized oxygen vacancies [30]. This indicates that a more resistive grain boundary is dominating the total response, which agrees well with the exceptionally high resistivity calculated from the hysteresis loops.

In this scenario, the possibility of a screening of the electric field within the grains by the grain boundaries needs to be considered when discussing the size effects reported. Actually, ferroelectric switching moving away of saturation when decreasing grain size might be attributed to a grain boundary effect, and so might be the depletion of the dielectric anomaly associated with the ferroelectric transition. The grain boundary effect must be also considered to understand the mechanisms behind the behavior of the dielectric permittivity for the nanostructured ceramic with the smallest grain size, G = 28 nm. In this case, the dielectric anomaly vanishes, as observed in figure 3, either because of the disappearance of the ferroelectric transition or because of its severe depletion, considering the exceptionally high grain boundary resistivity of this ceramic.

As the first option is directly associated with a loss of the ferroelectric character, local piezoelectric measurements were carried out by PFM in this ceramic to clarify whether this material still retains its ferroelectricity. Figure 7(a) shows a phase PFM image (out-of-plane component) in which ferroelectric domains with an average size similar to the grain size are clearly observed, thus indicating that the polar state does persist and also that nanometric grains are typically monodomains. Besides, a representative in-field piezoelectric hysteresis

loop is shown in figure 7(b), giving experimental evidence of local switching and thus of ferroelectricity in this nanostructured ceramic.

The absence of macroscopic ferroelectric switching is usually attributed to the pinning of transgranular 180° domains at the grain boundaries, as suggested for nanostructured ceramics of $BaTiO_3$ [3, 4]. However, the exceptionally high resistivity of the grain boundaries in the BSPT ceramic with the smallest grain size must play an important role. If, as a consequence of this, the electric field within the grains is effectively screened by the grain boundaries, the value of the external bias field required to achieve macroscopic switching of the whole ceramic may be above the one that causes dielectric breakdown, and thus macroscopic P-E hysteresis loops are not attainable. Besides, vanishes of the dielectric anomaly associated with the ferroelectric transition cannot be explained by the loss of the ferroelectric character below a certain critical crystal size, but must be attributed to its severe depletion. This result indicates that other effects inherent to the nature of the ceramic material must be considered when determining the critical grain size below which ferroelectricity vanishes in polycrystals.

4. Conclusions

The macroscopic electrical properties of dense, nanostructured ceramics of $0.375BiScO_3$-$0.625PbTiO_3$ are strongly influenced by highly resistive grain boundaries. It is proposed that the screening of the electric field within the grains by the grain boundaries makes gradually difficult polarization switching in the material as the grain size decreases, though individual grains still maintain the ability of local switching as demonstrated by PFM, even for the ceramic with the smallest average grain size of 28 nm. This is must probably also responsible of the depletion of the dielectric anomaly associated with the ferroelectric transition, which even disappears for the nanostructured ceramic with the smallest grain size.

Acknowledgments

This work was supported by the MICINN (Spain) through the projects MAT2007-61884 and MAT2008-02003/NAN. Drs. H. Amorín and T. Hungría thank financial support by the MICINN (Ramón y Cajal Programme) and CSIC (JAEDOC082 Contract), respectively. Authors gratefully acknowledge Dr. J. Galy (CEMES-CNRS and PNF2, Toulouse) for his support in the processing of the nanostructured materials by SPS. Technical support by Ms. I. Martínez from ICMM-CSIC is also acknowledged.

References

[1] Setter N and Waser R 2000 *Acta Mater.* **48** 151

[2] Setter N, Damjanovic D, Eng L, Fox G, Gevorgian S, Hong S, Kingon A, Kohlstedt H, Park N Y, Stephenson G B, Stolitchnov I, Taganstev A K, Taylor D V, Yamada T and Streiffer S 2006 *J. Appl. Phys.* **100** 051606

[3] Buscaglia M T, Buscaglia V, Viviani M, Petzelt J, Savinov M, Mitoseriu L, Testino A, Nanni P, Harnagea C, Zhao Z and Nygren M 2004 *Nanotechnology* **15** 1113

[4] Buscaglia M T, Viviani M, Buscaglia V, Mitoseriu L, Testino A, Nanni P, Zhao Z, Nygren M, Harnagea C, Piazza D and Galassi C 2006 *Phys. Rev. B* **73** 064114

[5] Zhang H T, Yan H X, Ning H P, Reece M J, Eriksson M, Shen Z J, Kan Y M and Wang P L 2009 *Nanotechnology* **20** 385708

[6] Carreaud J, Gemeiner P, Kiat J M, Dkhil B, Bogicevic C, Rojac T and Malic B 2005 *Phys. Rev. B* **72** 174115

[7] Algueró M, Hungría T, Amorín H, Ricote J, Galy J and Castro A 2007 *Small* **3** 1906

[8] Jiménez R, Amorín H, Ricote J, Carreaud J, Kiat J M, Dkhil B, Holc J, Kosec M and Algueró M 2008 *Phys. Rev. B* **78** 094103

[9] Amorín H, Jiménez R, Hungría T, Castro A and Algueró M 2009 *Appl. Phys. Lett.* **94** 152902

[10] Bovtun V, Kamba S, Veljko S, Nuzhnyy D, Kroupa J, Savinov M, Vaněk P, Petzelt J, Holc J, Kosec M, Amorín H and Algueró M 2009 *Phys. Rev. B* **79** 104111

[11] Randall C A, Kim N, Kucera J P, Cao W and Shrout T R 1998 *J. Am. Ceram. Soc.* **81** 677

[12] Zhang L, Zhong W L, Wang C L, Zhang P L and Wang Y G 1999 *J. Phys. D: Appl. Phys.* **32** 546

[13] Buixaderas E, Bovtun V, Kempa M, Savinov M, Nuzhnyy D, Kadlec F, Vaněk P, Petzelt J, Eriksson M and Shen Z 2010 *J. Appl. Phys.* **107** 014111

[14] Eitel R E, Randall C A, Shrout T R and Park S E 2002 *Jpn. J. Appl. Phys.* **41** 2099

[15] Zhang S J, Randall C A and Shrout T R 2003 *Appl. Phys. Lett.* **83** 3150

[16] Zhang S J, Eitel R E, Randall C A, Shrout T R and Alberta E F 2005 *Appl. Phys. Lett.* **86** 262904

[17] Chaigneau J, Kiat J M, Malibert C and Bogicevic C 2007 *Phys. Rev. B* **76** 094111

[18] Hungría T, Houdellier F, Algueró M and Castro A 2010 *Phys. Rev. B* **81** 100102

[19] Zou T T, Wang X H, Wang H, Zhong C F, Li L T and Chen I W 2008 *Appl. Phys. Lett.* **93** 192913

[20] Zou T T, Wang X H, Zhao W and Li L T 2008 *J. Am. Ceram. Soc.* **91** 121

[21] Algueró M, Amorín H, Hungría T, Galy J and Castro A 2009 *Appl. Phys. Lett.* **94** 012902

[22] Algueró M, Ricote J, Hungría T and Castro A 2007 *Chem. Mater.* **19** 4982

[23] Hungría T, Galy J and Castro A 2009 *Adv. Eng. Mater.* **11** 615

[24] Chen A, Zhi Y and Cross L E 2000 *Phys. Rev B* **62** 228

[25] Hungría T, Amorín H, Galy J, Ricote J, Algueró M and Castro A 2008 *Nanotechnology* **19** 155609

[26] Amorín H, Ricote J, Jiménez R, Holc J, Kosec M and Algueró M 2008 *Scripta Mater.* **58** 755

[27] West A R, Sinclair D C and Hirose N 1997 *J. Electroceram.* **1** 65

[28] Mahajan S, Thakur O P, Bhattacharya D K and Sreenivas K 2009 *J. Phys. D: Appl. Phys.* **42** 065413

[29] Singh G and Tiwaria V S 2009 *J. Appl. Phys.* **106** 124104

[30] Mestric H, Eichel R A, Dinse K P, Ozarowski A, van Tol J, Brunel L C, Kungl H, Hoffmann M J, Schonau K A, Knapp M and Fuess H 2006 *Phys. Rev B* **73** 184105

Table 1. Correlation between SPS conditions, average grain size (G) and macroscopic properties of the BSPT ceramics. d_{33} is the piezoelectric coefficient and ρ is the total resistivity calculated from the low-field hysteresis loops at 0.1 Hz. Results on a coarse grain ceramic (CGC) prepared by conventional sintering are included for comparison.

SPS conditions	G	d_{33} (pm/V)	ρ (Ω·cm)
650 ºC / 120 MPa / 3 min	28 nm	2 ± 1	2.2×10^{12}
650 ºC / 75 MPa / 3 min	80 nm	24 ± 2	9.6×10^{10}
800 ºC / 75 MPa / 3 min	375 nm	110 ± 5	4.6×10^{10}
CGC 1100 ºC / 1 h	3 μm	150 ± 5	3.7×10^{10}

Figure captions

Figure 1. TEM image and grain size distribution of the nanostructured BSPT ceramic with an average grain size of 28 nm obtained by SPS at 650 ºC / 120 MPa / 3 min.

Figure 2. XRD patterns of BSPT ceramics with average grain sizes of (a) 28 nm (b) 80 nm and (c) 375 nm. Miller indexes refer to the perovskite structure.

Figure 3. Temperature dependence of the relative dielectric permittivity (K') for BSPT ceramics with average grain sizes of (**1**) 28 nm (**2**) 80 nm and (**3**) 375 nm. The arrows indicate the direction of increasing frequency from 100 Hz to 1 MHz.

Figure 4. Temperature dependence of the dielectric dissipation factor (tan δ) for BSPT ceramics with average grain sizes of (**1**) 28 nm (**2**) 80 nm and (**3**) 375 nm. The arrows indicate the direction of increasing frequency from 100 Hz to 1 MHz.

Figure 5. (a) P-E hysteresis loops and (b) spontaneous (P_s), remnant (P_r) polarizations vs maximum applied electric field for BSPT ceramics with average grain sizes of (**1**) 28 nm, (**2**) 80 nm, (**3**) 375 nm, and (**4**) for the coarse grain ceramic.

Figure 6. (a) Temperature dependence of *dc* conductivity (σ_{dc}) for BSPT ceramics with average grain sizes of (**1**) 28 nm, (**2**) 80 nm, and (**3**) for the coarse grain ceramic. E_a is the activation energy. (b) Frequency dependence of the *ac* conductivity (σ_{ac}) for the BSPT ceramic with an average grain size of 375 nm. The arrow indicates increasing temperature from 220 to 500 ºC. The small arrows indicate the approximate position of the high frequency contribution to σ_{ac}.

Figure 7. (a) Phase PFM image (out-of-plane component) and (b) piezoresponse under bias field for the nanostructured BSPT ceramic with an average grain size of 28 nm.

Fig. 1. H. Amorín et al.

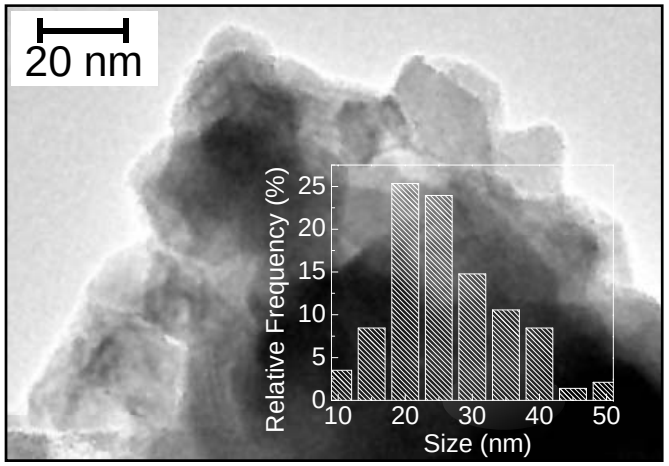

Fig. 2. H. Amorín et al.

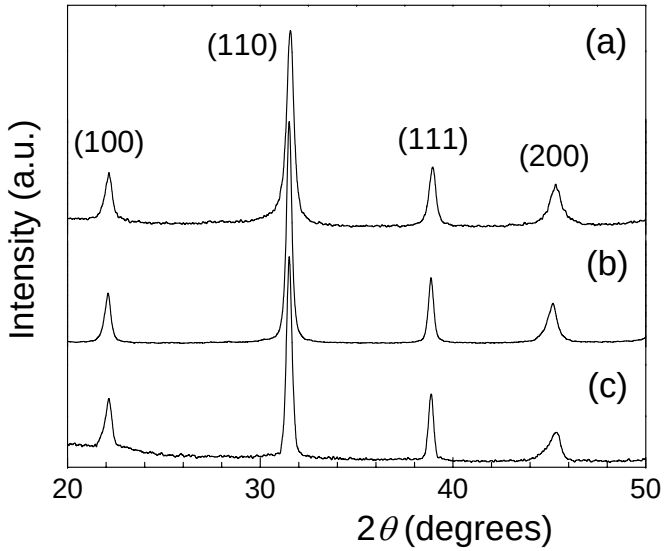

Fig. 3. H. Amorín et al.

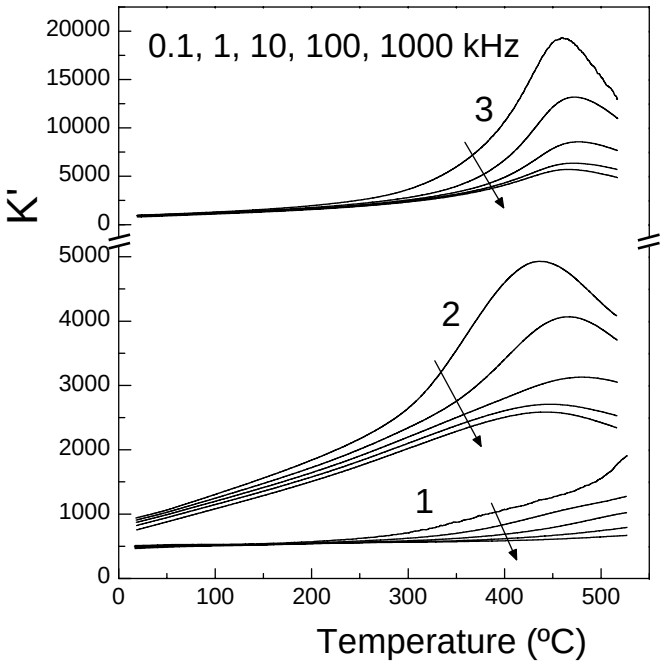

Fig. 4. H. Amorín et al.

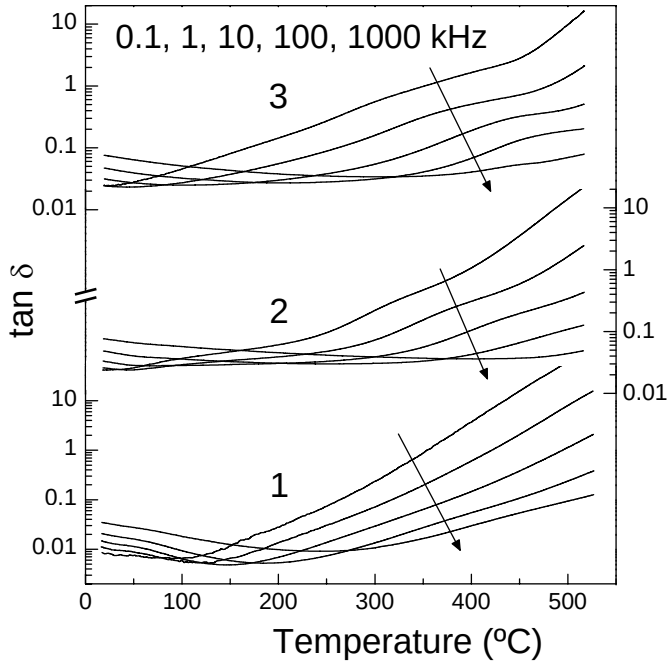

Fig. 5. H. Amorín et al.

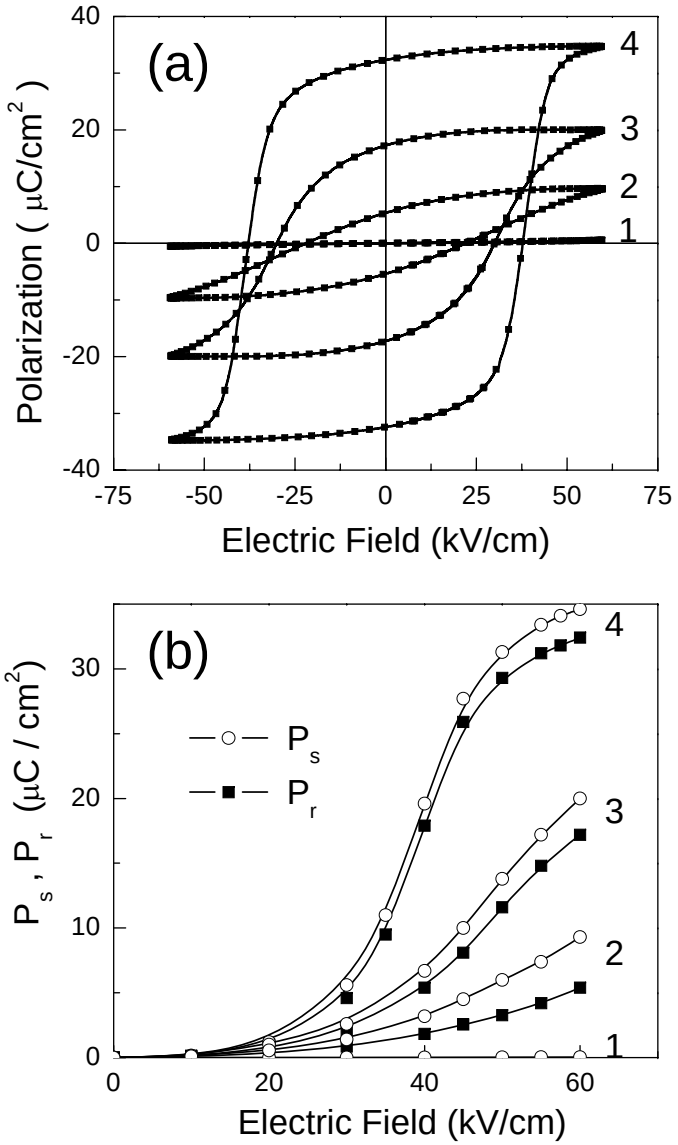

Fig. 6. H. Amorín et al.

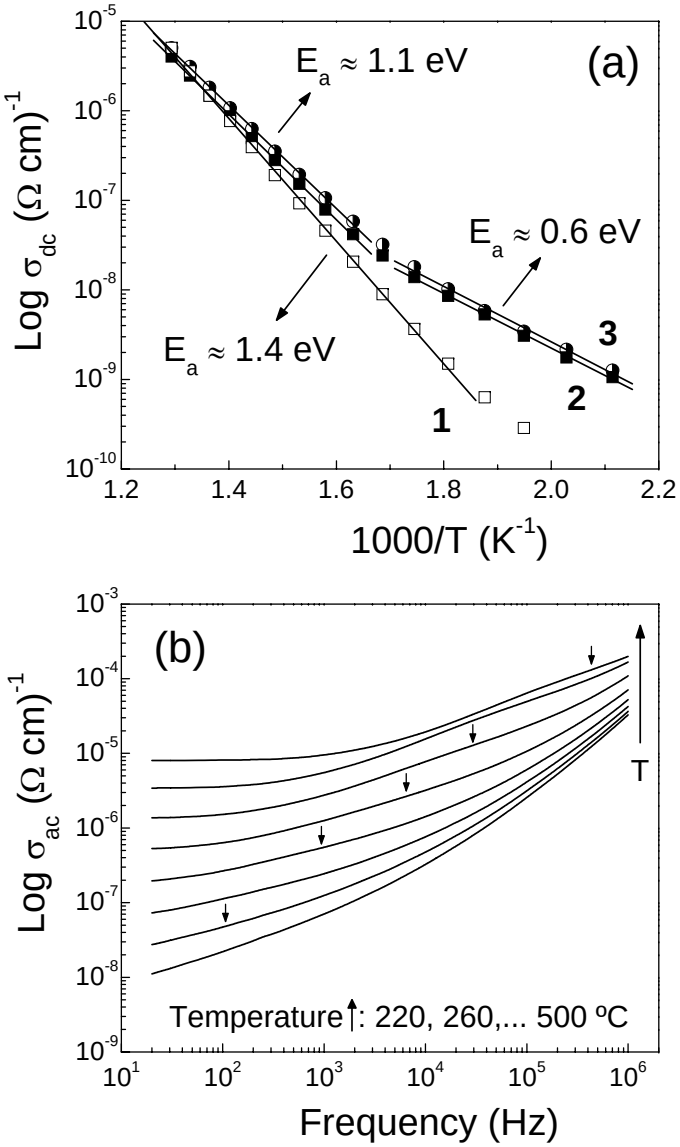

Fig. 7. H. Amorín et al.